

Estimating surface fluxes over middle and upper streams of the Heihe River Basin with ASTER imagery

Weiqliang Ma¹, Yaoming Ma^{2, 1}, Zeyong Hu¹, Bob Su³, Jiemin Wang¹, and Hirohiko Ishikawa⁴

1. Laboratory for Climate Environment and Disasters of Western China, Cold and Arid Regions Environmental and Engineering Research Institute, Chinese Academy of Sciences, Lanzhou, Gansu 730000, China.
2. Laboratory of Tibetan Environment Changes and Land Surface Processes, Institute of Tibetan Plateau Research, Chinese Academy of Sciences, Beijing, China.
3. International Institute for Geo-Information Science and Earth Observation, Enschede, Netherlands
4. Disaster Prevention Research Institute, Kyoto University, Kyoto, Japan.

E-mail: wqma@lzb.ac.cn

Abstract

Surface fluxes are important boundary conditions for climatological modeling and the Asian monsoon system. Recent availability of high-resolution, multi-band imagery from the ASTER (Advanced Space-borne Thermal Emission and Reflection Radiometer) sensor has enabled us to estimate surface fluxes to bridge the gap between local scale flux measurements using micrometeorological instruments and regional scale land-atmosphere exchanges of water and heat fluxes that are fundamental for the understanding of the water cycle in the Asian monsoon system. In order to evaluate of Surface Energy Balance System (SEBS) algorithm applicable in an arid and cold environment, SEBS method based on ASTER data and field observations has been proposed and tested for deriving net radiation flux (R_n), soil heat flux (G_0), sensible heat flux (H) and latent heat flux (λE) over heterogeneous land surface in this paper. As a case study, the methodology was applied to the experimental area of the WATER (Watershed Allied Telemetry Experimental Research), located at the mid-to-upstream sections of the Heihe River, northwest China. The ASTER data of 3 May and 4 June in 2008 with clear-sky conditions was used in this paper for the case of mid-to-upstream sections of the Heihe River Basin. To validate the proposed methodology, the ground-measured land surface heat fluxes (net radiation flux (R_n), soil heat flux (G_0), sensible

heat flux (H) and latent heat flux (λE) were compared to the ASTER derived values. The results show that the derived surface variables and land surface heat fluxes in different months over the study area are in good accordance with the land surface status. It is therefore concluded that the proposed methodology is successful for the retrieval of land surface heat fluxes using the ASTER data (L1B) and field observation over the study area.

1 Introduction

Among many land surface experiments having been carried out so far, arid and cold regions were paid little attention. The land surface observations in arid and cold regions, both remotely sensed and in-situ, need to be strengthened for a better understanding of hydrological and ecological processes at different scales. The Watershed Allied Telemetry Experimental Research (WATER) is a simultaneous air-borne, satellite-borne, and ground-based remote sensing experiment conducted in the Heihe Basin, the second largest inland river basin in the northwest arid regions of China. The WATER is aiming at the research on water cycles, eco-hydrological and other land surface processes in catchment-scale. Data sets with high-resolution and spatiotemporal consistency will be generated based on this experiment. An integrated watershed model and a catchment-scale land/hydrological data assimilation system is proposed to be developed. The mission of WATER is to improve the observability, understanding, and predictability of hydrological and related ecological processes at catchment scale, accumulate basic data for the development of watershed science and promote the applicability of quantitative remote sensing in watershed science studies (Li, X., 2009).

Remote sensing offers the possibility to derive regional distribution of land surface heat fluxes over heterogeneous land surface in combination with sparse field experimental stations. Remote sensing data provided by satellites are a means of obtaining consistent and frequent observations of spectral albedo and emittance of radiation at elements in a patch landscape and on a global scale (Sellers et al., 1990). The land surface variables, such as surface temperature T_{sfc} , surface hemispherical albedo r_0 , Normalized Difference Vegetation Index ($NDVI$), Modified Soil adjusted Vegetation index ($MSAVI$), Leaf Area index (LAI) and surface thermal emissivity ϵ can be derived directly from satellite observations (e.g., Susskind et al., 1984; Che'din et al., 1985; Tucker, 1986; Wan and Dozier, 1989; Menenti et al., 1989; Becker and Li, 1990, 1995; Watson et

al., 1990; Baret and Guyot, 1997; Price, 1992; Kahle and Alley, 1992; Li and Becker, 1993; Qi et al., 1994; Schmugge et al., 1995; Sobrino and Raissouni, 2000; Ma et al., 2003a; Ma et al., 2003b; Kato, 2005; Ma, 2006b, 2007, 2009). The regional heat fluxes can be determined indirectly with the aid of these land surface variables (Pinker, 1990).

Studies have explored several approaches to estimate the regional distribution of surface heat fluxes in recent years. These methods require specification of the vertical temperature difference between the surface temperature and the air temperature and an exchange resistance (e.g., Kustas et al., 1989; Kustas, 1990; Wang et al., 1995; Menenti et al., 1991; Menenti and Choudhury, 1993; Bastiaanssen, 1995; Kustas and Norman, 1997; Su, 2002; Jia et al., 2003). However, these remote sensing retrieval methods have been performed in homogeneous moist or semiarid regions, and investigations in heterogeneous landscape of arid and cold regions (e.g., the WATER area) are rare or limited.

NOAA/AVHRR (the National Oceanic and Atmospheric Administration/Advanced Very High Resolution Radiometer), GMS (Geostationary Meteorological Satellite) and Landsat-7 ETM (Enhanced Thematic Mapper) data were used to determine regional land surface heat fluxes over heterogeneous landscape of the Tibetan Plateau (Ma et al., 2003a; Ma et al., 2003b; Ma et al., 2005; Ma et al., 2006; Oku et al., 2007). However, the resolution of the NOAA/AVHRR and GMS data is about $1\text{km}\times 1\text{km}$ and sub-pixel heterogeneity has been omitted. So have Landsat-7 ETM data. The aim of this research is to upscale in-situ point observations of land surface variables and land surface heat fluxes to the regional scale using high-resolution ($15\text{m}\times 15\text{m}$) ASTER data.

2 Data

2.1 Ground measurements

WATER is a simultaneous airborne, satellite-borne, and ground-based remote sensing experiment taking place in the Heihe River Basin, the second largest inland river basin in the arid regions of northwest China. WATER is first of all a multiscale land surface/hydrological experiment in a cold and arid region. In this paper, Yingke, Huazhaizi, Guantan, Maliantan, A'rou, Binggou and Yakou are selected as the middle and upper streams of the Heihe River Basin weather stations. Yingke oasis station, located to the south of Zhangye city, is a typical irrigated farmland. The primary crops are maize and wheat. Huazhaizi station is located on desert steppe to

the south of Zhangye oasis. Guantan is a forest station in the south of Zhangye oasis. Maliantan is grassland station near Guantan station. A'rou station is located in the middle reaches of the Babao River Basin and is a relatively flat area with a mean elevation of about 3000 m. The seasonally frozen soil is widely distributed. Binggou station is a high-mountain drainage system and the mean depth of the seasonal snowpack is about 0.5 m, with a maximum of 0.8–1.0 m. The lower limit of permafrost is about 3400 m. Yakou station is mountain pass. These stations represent the middle and upper streams of the Heihe River Basin characteristics. In order to compare these stations observation results, all instruments are demarcated before the experiments. Their details are listed in Table 1 and Figure 1 (Li, X., 2009).

Table 1. Ground measurements items in WATER area

Name	Location	Items	Land surface character
Yingke	100°25' E, 38°51' N, 1519 m	wind speed, air temperature and humidity (3 and 10 m), wind direction, air pressure precipitation, four components of radiation, and LST. soil: temperature and moisture profile (10, 20, 40, 80, 120, and 160 cm), and heat flux (5 and 15 cm). EC.	Cropland(maize)
Huazhaizi	100°19' E, 38°46' N, 1726 m	wind speed, air temperature and humidity (2 and 10 m), wind direction, air pressure, precipitation, four components of radiation, and LST. soil: temperature and moisture profile (5, 10, 20, 40, 80, and 160 cm), and heat flux (5 and 15 cm).	Desert steppe
Guantan	100°15' E, 38°32' N, 2835 m	wind speed, air temperature and humidity (2, 10, and 24 m), four components of radiation (1.68 and 19.75 m), wind direction, air pressure, precipitation, snow depth, and PAR. soil: temperature and moisture profile (5, 10, 20, 40, 80, and 120 cm), frost depth, and heat flux (5 and 15 cm). EC, sap flow (3), fall-through, stemflow.	forest
Maliantan	100°18' E, 38°33' N, 2817 m	wind speed, air temperature and humidity (2 and 10 m), wind direction, air pressure, precipitation, and four components of radiation. soil: temperature and moisture profile (5, 10, 20, 40, 80, and 120 cm) and heat flux (5 and 15 cm).	Grassland
A'rou	100°27' E, 38°03' N, 3033m	wind speed, air temperature and humidity (2 and 10 m), wind direction, air pressure, precipitation, and four components of radiation.a soil: temperature, moisture, water potential profile (10, 20, 40, 80, 120, and 160 cm), and heat flux (5 and 15 cm). EC, LAS.	Alpine meadow
Binggou	100°13' E, 38°04' N, 3407m	wind speed, air temperature and humidity (2 and 10 m), wind direction, air pressure, precipitation, and four components of radiation. soil: temperature and moisture profile (5, 10, 20, 40, 80, and 120 cm) and heat flux (5 and 15 cm).	Alpine marshy meadow
Yakou	100°14' E, 38°01' N, 4101 m	wind speed, air temperature and humidity (2 and 10 m), wind direction, air pressure, precipitation, snow depth, and four components of radiation. soil: temperature and moisture profile (5, 10, 20, 40, 80, and 120 cm) and heat flux (5 and 15cm).	Cold desert

2.2 Satellite data

The recent study of high-resolution, multi-band imagery from the ASTER sensor has enabled

us to estimate surface fluxes. ASTER covers a wide spectral region with 14 bands from the visible to the thermal infrared with high spatial, spectral and radiometric resolution. The spatial resolution varies with wavelength: 15m in the visible and near-infrared bands (VNIR, 0.52–0.86 μm), 30m in the short wave infrared bands (SWIR, 1.6-2.43 μm), and 90m in the thermal infrared bands (TIR, 8.1–11.6 μm) (Yamaguchi, 1998). The level of ASTER data is L1B.

The most relevant data, collected at the WATER (Figure 1) surface stations to support the parameterization of land surface heat fluxes and analysis of ASTER images in this paper, consist of surface radiation budget components, surface radiometric temperature, surface albedo, humidity, wind speed and direction measured at the Atmospheric Boundary Layer (ABL) towers, Automatic Weather Stations (AWSs), turbulent fluxes measured by eddy correlation technique, soil heat flux, soil temperature profiles, soil moisture profiles, and the vegetation state. (Li, X., 2009).

3 Methodology

3.1 Theory and Scheme

3.1.1 Land surface data and energy character

The land surface data observed at three stations of WATER was processed using the combinatory method (Hu and Qi 1991) to determine sensible, latent, and soil heat flux. Calculation equations follow:

$$H_0 = \rho C_p \kappa^2 Z_A^2 \frac{\partial U}{\partial Z} \frac{\partial \theta}{\partial Z} \quad (1)$$

$$\lambda E_0 = \rho \lambda \kappa^2 Z_A^2 \frac{\partial U}{\partial Z} \frac{\partial q}{\partial Z} \quad (2)$$

$$Z_A = \sqrt{Z_i Z_{i+1}} \quad (3)$$

$$G_0 = G_z + \int_0^z C_s \frac{\partial T}{\partial t} dz \quad (4)$$

$$F = \frac{R_n - G_0}{H_0 + \lambda E_0} \quad (5)$$

$$H = H_0 F \quad (6)$$

$$\lambda E = \lambda E_0 F \quad (7)$$

Where H_0 and λE_0 are former sensible and latent heat flux, λ is latent heat of vaporization,

Z_A is geometric mean value between Z_i and Z_{i+1} , C_s is the volumetric heat capacity, G_z is the observed soil heat flux below z from the surface ($z=10\text{cm}$ was used here) and κ is *Karman* constant ($\kappa=0.4$). Here megadyne temperature (θ) and specific humidity (q) are:

$$\theta = T \left(\frac{1000}{p} \right)^{0.286} \quad (8)$$

$$q = \frac{0.622e}{p - 0.378e} \quad (9)$$

Where p is pressure and e is vapor pressure. Here $e = E \times RH$, E is saturation water vapor pressure and RH is relative humidity.

Using Eqns (1), (5) and (6) equations, sensible heat flux can be derived. In the same way, Eqns. (2), (5) and (7) can get latent heat flux. Soil heat flux can be obtained from Eq. (4) (Tanaka 2001).

In order to validate the results of combinatory method, the EC (eddy correlation) methodology is used here. The turbulence data, observed with a sonic anemometer-thermometer and an infrared hygrometer, was processed using the eddy correlation methodology. Some main calculation equations are

$$\text{Sensible heat flux} \quad H = \rho C_p \overline{w'T'} = -\rho C_p u_* T_* \quad (10)$$

$$\text{Latent heat flux} \quad \lambda E = \lambda \rho \overline{w'q'} = -\lambda \rho u_* q_* \quad (11)$$

Figure 2 shows the Yingke station's diurnal variations of surface heat fluxes on behalf of WATER area, including net radiation (R_n), sensible heat flux (H), latent heat flux (λE) and soil heat flux (G_0). It can be seen that: the diurnal variations of net radiation, sensible heat, latent heat and soil heat flux are obvious. They increase with the increasing of solar altitude angle after the sunrise in the morning, and the maximum appears around noon then they decrease with the decreasing of solar altitude angle. Taking one with another soil heat flux changes slowly and its value is the least one in the land surface energy budget. The energy balance closure is good for all the sites.

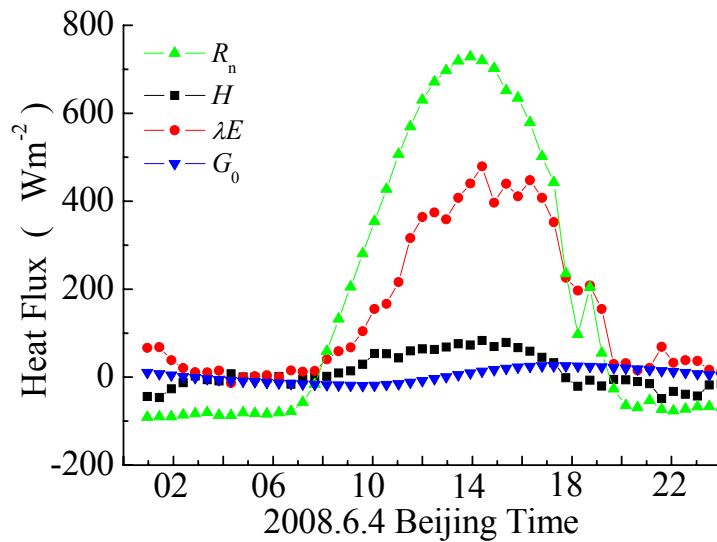


Figure 2. Diurnal variations of land surface heat fluxes

3.1.2 Remote sensing data

A Surface Energy Balance System (SEBS, Su, 2002) is proposed for the estimation of atmospheric turbulent fluxes and evaporative fraction using satellite earth observation data, in combination with meteorological information at proper scales. SEBS consists of: a set of tools for the determination of the land surface physical parameters, such as albedo, emissivity, temperature, vegetation coverage etc., from spectral reflectance and radiance measurements; a model for the determination of the roughness length for heat transfer (Su, 2002).

In this study, the SEBS retrieval algorithm is used for the ASTER data to evaluate of algorithm applicable in an arid and cold environment (Su, 2002). Firstly we resized the ASTER data in same resolution with bands VNIR, SWIR and TIR. The general concept of the methodology is shown in a diagram (Figure 3). NDVI can derive from band 2 and 3 of ASTER data. The surface albedo for shortwave radiation (r_0) is retrieved from narrowband-broadband conversion by Liang (Liang, 2000). The land surface temperature (T_{sfc}) is derived using a method developed by JIMENEZ-MUNOZ Juan C. (2006) from multispectral thermal infrared data. JIMENEZ-MUNOZ Juan C. (2006) also evaluated a technique to extract emissivity information from multispectral thermal infrared data adding vegetation information. The radiative transfer model SMAC (Rahman, H., and Dedieu, G., 1994) computes the downward shortwave and

longwave radiation at the surface. The input downward shortwave radiation is observation data from WATER AWS station. With these results the surface net radiation flux (R_n) is determined. On the basis of the field observations, the soil heat flux (G_0) is estimated from the net radiation flux (R_n). The sensible heat flux (H) is estimated from T_{sfc} , air temperature (T_a) and other parameters, and regional latent heat flux (λE) is derived as the residual of the energy budget theorem (Liou, 2004; Ma,2006) for land surface.

[Insert Figure 3 about here]

The net radiation flux R_n is estimated as

$$\begin{aligned} R_n(x, y) &= K_{\downarrow}(x, y) - K_{\uparrow}(x, y) + L_{\downarrow}(x, y) - L_{\uparrow}(x, y) \\ &= \{1 - r_0(x, y)\} \cdot K_{\downarrow}(x, y) + \varepsilon_0(x, y) \{L_{\downarrow}(x, y) - \sigma T_{sfc}^4(x, y)\} \end{aligned} \quad (1)$$

where $\varepsilon_0(x, y)$ is surface emissivity, $K_{\downarrow}(\text{Wm}^{-2})$ represents the downward shortwave (0.3–3 μm) and $L_{\downarrow}(\text{Wm}^{-2})$ is the downward longwave (3–100 μm) radiation components, respectively. Surface albedo $r_0(x, y)$ is derived from narrowband-broadband conversion method by Liang (2000). Since ASTER has nine bands, it is expected that so many bands should enable us to convert narrowband to broadband albedos effectively. Liang (2000) found that the conversions are quite linear. The resultant linear equations are collated in the following.

$$r_0 = 0.484\alpha_1 + 0.335\alpha_3 - 0.324\alpha_5 + 0.551\alpha_6 + 0.305\alpha_8 - 0.367\alpha_9 - 0.0015 \quad (2)$$

Where $i(i=1-9)$ are the correspondent ASTER band surface reflectance.

The equation to calculate soil heat flux is parameterized as (Su, 2002):

$$G_0 = R_n[\Gamma_c + (1 - f_c) \bullet (\Gamma_s - \Gamma_c)] \quad (3)$$

in which it is assumed that the ratio of soil heat flux to net radiation $\Gamma_c = 0.05$ for full vegetation canopy (Monteith,1973) and $\Gamma_s=0.315$ for bare soil (Kustas and Daughtry, 1989). An interpolation is then performed between these limiting cases using the fractional canopy coverage, f_c . In this study, we try to use the constant to the Heihe River.

In order to derive the sensible and latent heat flux, the similarity theory will be made use of. In ASL (Atmospheric Surface Layer), the similarity relationships for the profiles of the mean wind speed, u , and the mean temperature difference between the surface and the air, $\theta_0 - \theta_a$, are usually written in integral form as

$$u = \frac{u_*}{k} \left[\ln \left(\frac{z-d_0}{z_{om}} \right) - \Psi_m \left(\frac{z-d_0}{L} \right) + \Psi_m \left(\frac{z_{om}}{L} \right) \right] \quad (4)$$

$$\theta_0 - \theta_a = \frac{H}{ku_* \rho C_p} \left[\ln \left(\frac{z-d_0}{z_{oh}} \right) - \Psi_h \left(\frac{z-d_0}{L} \right) + \Psi_h \left(\frac{z_{oh}}{L} \right) \right] \quad (5)$$

where z is the height above the surface, u_* is the friction velocity, C_p is specific heat of air at constant pressure, ρ is the density of air, $k = 0.4$ is von Karman's constant, d_0 is the zero plane displacement height, z_{om} is the roughness height for momentum transfer, θ_0 is the potential temperature at the surface, θ_a is the potential air temperature at height z , z_{oh} is the scalar roughness height for heat transfer, Ψ_m and Ψ_h are the stability correction functions for momentum and sensible heat transfer respectively, and L is the Obukhov length defined as:

$$L = \frac{\rho C_p u_*^3 \theta_v}{kgH} \quad (6)$$

where g is the acceleration due to gravity and θ_v is the virtual potential temperature near the surface.

The latent heat flux λE is the residual resulting from an application of the energy budget theorem to the land surface :

$$\lambda E = R_n - H - G_0 \quad (7)$$

3.2 Retrieval of land surface parameters

Vegetation plays an important role in the interaction of air-land over WATER area, this will require to understand or estimate vegetation variables in temporal and regional scale. As satellite can observe the global surface continuously from space, remote sensing will be a useful tool in monitoring or studying the vegetation variation. Since the launch of the first earth resources satellite in 1972, remarkable efforts have been made to establish a close relationship between radiometric information and vegetation covers. Generally, these bands are present on meteorological and earth observation satellites and often contain more than 90% of the information relating to vegetation (Beret et al., 1988). The different combinations between these channels are called vegetation variables. In the area of applications and research in satellite remote sensing, over forty vegetation variables have been developed during the last three decades. The more common and useful vegetation indices are including Normalized Difference Vegetation Index (NDVI) and vegetation coverage P_v (or fractional vegetation cover f_c).

3.2.1 NDVI

Because chlorophyll has a strong spectral absorption in the visible region (Tucker, 1986), land surface spectral reflectance provide information on the presence of chlorophyll and thus on surface vegetation conditions. This information can be utilized to calculate the NDVI for each pixel from the radiances in the red and infrared channels. For ASTER data, NDVI proposed as:

$$NDVI(x, y) = \frac{band3 - band2}{band3 + band2} \quad (8)$$

where band3 is the ASTER reflectance in the red channel, band2 is the ASTER reflectance in the near infrared channel.

3.2.2 Vegetation coverage P_v

Vegetation coverage P_v is the proportion of vegetation. Carlson and Ripley (1997) proposed P_v as

$$P_v(x, y) = \left[\frac{NDVI(x, y) - NDVI_{min}}{NDVI_{max} - NDVI_{min}} \right]^2 \quad (9)$$

where $NDVI_{min}$ and $NDVI_{max}$ are the NDVI values for bare soil and full vegetation respectively.

3.3 Case Studies and Validation

As a case study, four scenes of ASTER data over the mid-to-upstream sections of the Heihe River Basin are used. ASTER observation time is 12:19 using Beijing time. Figure 4 shows the distribution maps of surface heat fluxes around the WATER area. Figure 5 shows the validation of the derived net radiation R_n , soil heat flux G_0 , sensible heat flux H and latent heat flux λE against ground measurements at the WATER stations, the averaging time is 10 minutes with each plot of ground measurements. Yingke, Huazhaizi, Guantan, Maliantan, A'rou, Binggou and Yakou with 1:1 line.

[Insert Figure 4 about here]

[Insert Figure 5 about here]

The results show the following:

1. The derived surface heat fluxes (net radiation flux R_n , soil heat flux G_0 , sensible heat flux H and latent heat flux λE) in different months over the study area are in good accordance with the land surface status. The experimental area includes a variety of land surfaces, such as a large area

of grassy marshland, some desertification grassland areas, many small rivers; therefore these derived parameters show a wide range due to the strong contrast of surface features. For example, in Yingke station it is cropland (maize) in summer. So the latent heat flux shows the main parts of land surface flux. To the contrary the sensible heat flux shows the main parts of land surface flux in Huazaizi station because it is the desert steppe. (Figure 4).

2. The derived net radiation flux over the study area is very close to the field measurement. It is the result of the improvement on surface albedo and surface temperature. Surface albedo is derived from narrowband-broadband conversion method by Liang (2000). Since ASTER has nine bands, it is expected that so many bands should enable us to convert narrowband to broadband albedos effectively. Liang (2000) found that the conversions are quite linear.

3. The derived regional sensible heat flux and latent heat flux at the validation sites in the WATER area is in good agreement with field measurements (Figure 5). This is due to the fact that atmospheric boundary layer processes have been considered in more detail in our methodology and the proposed parameterization for sensible heat flux can be used over the upper streams of the Heihe River Basin area. Latent heat flux is in good agreement with field measurement because of adequate parameterization of net radiation flux R_n , soil heat flux G_0 , sensible heat flux H .

4. Concluding remarks

In this study, the regional distributions of land surface heat fluxes (net radiation flux, soil heat flux, sensible heat flux and latent heat flux) over middle and upper streams of the Heihe River Basin were derived with the aid of ASTER data and field observations. Reasonable results of land surface heat fluxes were gained in this study.

The retrieval of regional land surface heat fluxes over heterogeneous landscape is not an easy task.

1. Only four ASTER images are used in this study. To obtain more accurate regional land surface fluxes (daily to seasonal variations) over a larger area (the Heihe River Basin), more field observations (ABL tower and radiation measurement system, radiosonde system, turbulent fluxes measured by eddy correlation technique, soil moisture and soil temperature measurement system etc.) and other satellite sensors such as MODIS (Moderate Resolution Imaging Spectroradiometer) and NOAA/AVHRR with more frequent temporal coverage have to be used.

2. This study implies the SEBS method is only applicable to clear-sky days (SEBS, as an algorithm of estimating land surface turbulent fluxes, can also be used for cloudy days if the land surface parameters can be derived from the satellite observations somehow.). However optical remote sensing is affected by clouds. In order to extend its applicability to cloudy skies, we should consider using microwave remote sensing data to derive surface temperature and other land surface variables.

SEBS has been developed to estimate atmospheric turbulent fluxes using satellite earth observation data, in combination with meteorological data from a proper reference height given by either in-situ measurements for application to a point, and radiosonde or meteorological forecasts for application at larger scales. On the basis of these experimental validations, SEBS can be used to estimate turbulent heat fluxes at different scales with acceptable accuracy.

Acknowledgments: This work was under the CAS Action Plan for West Development Program (KZCX2-XB2-09-04), “Quantitative Remote Sensing of Key Land Surface Parameters and Data Assimilation” project (KZCX2-YW-Q10-2) and Young Talent Project of the CAS (KZCX2-YW-QN309). Chinese State Key Basic Research Project (2005CB422003 and 2007CB714400). The auspices of the National Natural Science Foundation of China (40705004, 40825015 and 40810059006), the Key Projects of International Cooperation, CAS (GJHZ0735), EU-FP7 project “CEOP-AEGIS” and the Opening Foundation of Institute of Plateau Meteorology, CMA(LPM2007014). Special thanks are given to the two reviewers and the editor for very constructive comments.

References

- Baret, F., Guyot, G. , Teres, J.M. and Rigal, D. 1988, Profile spectral et estimation de la biomass. Proceeding of 4th International Colloquium on Spectral Signatures of Objects in Remote Sensing, Aussois, France, 93-98.
- Baret, F., and G. Guyot (1997), Potentials and limits of vegetation indices for LAI and APAR assessment, *Remote Sens. Environ.*, 35, 161– 173.
- Bastiaanssen, W. G. M., (1995), Regionalization of surface fluxes and moisture indicators in composite terrain, PhD Thesis, Wageningen Agric. Univ., Wageningen, Netherlands, 273pp.
- Bastiaanssen, W. G. M. (1995), Regionalization of Surface Flux Densities and Moisture Indicators in Composite Terrain, Ph.D. thesis, pp.143–161, Wageningen Agric. Univ., Wageningen, Netherlands.
- Becker, F., and Z.-L. Li (1995), Surface temperature and emissivity at various scales: Definition, measurement and related problems, *Remote Sens. Rev.*, 12, 225–253.
- Berk, A., L. S. Bernstein, and D. C. Robertson (1989), MODTRAN: A moderate resolution model for LOTRAN-7, GL-TR-89-0122, Geophys. Lab., Hanscom Air Force Base, Mass.
- Carlson, T.N., and Ripley, D.A., 1997, On the relation between NDVI, fractional vegetation cover, and leaf area index. *Remote Sensing of Environment*, 62: 241-252.
- Che'din, A., N. A. Scott, C. Wahiche, and P. Moulinier (1985), The improved initialisation inversion method: A high resolution physical method for temperature retrievals from Tiros-N series, *J. Clim. Appl. Meteorol.*, 24, 124–143.
- Hu Y, Qi Y (1991) The combinatory method to determine the turbulent fluxes and the universal functions in the surface layer. *ACTA Meteorologica Sinica*, 49(1):46-53 (in Chinese with English abstract)
- Jia, L., Su, Z., van den Hurk, B. J.J.M., Menenti, M., et al, 2003, Estimation of sensible heat flux using the Surface Energy Balance System (SEBS) and ATSR measurements, *Journal of Physics and Chemistry of the Earth*, 8: 75-88.

- JIMENEZ-MUNOZ Juan C., Sobrino, J., Gillespie, A., et al., (2006), Improved land surface emissivities over agricultural areas using ASTER NDVI, *Remote Sensing of Environment*, 103, 474–487
- K.N.Liou (2004), *An introduction to atmospheric radiation*(Second Edition), China Meteorol. Press, Beijing, China.
- Kahle, A. B., and R. E. Alley (1992), Separation of temperature and emittance in remotely sensed radiance measurements, *Remote Sens. Environ.*, 42, 107– 112.
- Kato, S, Y. Yamaguchi(2005), Analysis of urban heat-island effect using ASTER and ETM+ Data: Separation of anthropogenic heat discharge and natural heat radiation from sensible heat flux, *Remote Sensing of Environment*, 99: 44 – 54
- Kustas, W. P. (1990), Estimates of evapotranspiration with a one- and twolayer model of heat transfer over partial canopy cover, *J. Appl. Meteorol.*, 29, 704– 715.
- Kustas, W. P., and C. S. T. Daughtry (1990), Estimation of the soil heat flux/net radiation ratio from spectral data, *Agric. For. Meteorol.*, 39, 205– 223.
- Kustas,W. P., B. J. Choudhury, M. S. Moran, R. J. Reginato, R. D. Jackson, L. W. Gay, and H. L. Weaver, (1989), Determination of sensible heat flux over sparse canopy using thermal infrared data, *Agric. For. Meteorol.*, 44,197– 216.
- Li, X., et al. (2009), Watershed Allied Telemetry Experimental Research, *J. Geophys. Res.*, 114, D22103, doi:10.1029/2008JD011590.
- Li, Z.-L., and F. Becker (1993), Feasibility of land surface temperature and emissivity determination from AVHRR data, *Remote Sens. Environ.*, 43, 67– 85.
- Liang, S. Narrowband to broadband conversions of land surface albedo I Algorithms. *Remote Sensing of Environment*, 2000.Vol 76: 213-238
- Ma, W., (2007), Estimating regional heat surface fluxes over heterogeneous landscapes of the Tibetan Plateau by using ASTER data, PhD Thesis, Chinese Academy of Sciences.
- Ma, W., Ma, Y., (2006b), The annual variations on land surface energy in the northern Tibetan Plateau. *Environ. Geol.*, 50(5). doi:10.1007/s00254-006-0238-9
- Ma, W., Ma, Y., Li, M., et al, (2009), Estimating surface fluxes over the north Tibetan Plateau area with ASTER imagery, *Hydrol. Earth Syst. Sci.*, 13, 57-67

- Ma, Y., 2006, Determination of regional surface heat fluxes over heterogeneous landscapes by integrating satellite remote sensing with boundary layer observations, PhD Thesis, Wageningen University
- Ma, Y., H. Ishikawa, O. Tsukamoto, M. Menenti, Z. Su, T. Yao, T. Koike, and T. Yasunari (2003b), Regionalization of surface fluxes over heterogeneous landscape of the Tibetan Plateau by using satellite remote sensing, *J. Meteorol. Soc. Jpn.*, 81, 277– 293.
- Ma, Y., L. Zhong, Z. Su, H. Ishikawa, M. Menenti, and T. Koike (2006a), Determination of regional distributions and seasonal variations of land surface heat fluxes from Landsat-7 Enhanced Thematic Mapper data over the central Tibetan Plateau area, *Journal of Geophysics Research*, 111, D10305, doi:10.1029/2005JD006742.
- Ma, Y., Z. Su, T. Koike, T. Yao, H. Ishikawa, K. Ueno, and M. Menenti (2003a), On measuring and remote sensing surface energy partitioning over the Tibetan Plateau—From GAME/Tibet to CAMP/Tibet, *Phys.Chem. Earth*, 28, 63– 74.
- Menenti, M., and B. J. Choudhury (1993), Parameterization of land surface evaporation by means of location dependent potential evaporation and surface temperature range, in *Exchange Processes at the Land Surface for a Range of Space and Time Scales*, edited by H. J. Bolle, R. A. Feddes, and J. D. Kalma, IAHS Publ., 212, 561– 568.
- Menenti, M., W. G. M. Bastiaanssen, and D. Van Eick (1989), Determination of hemispheric albedo with Thematic Mapper data, *Remote Sens. Environ.*, 28, 327– 337.
- Menenti, M., W. G. M. Bastiaanssen, K. Hefny, and M. H. Abd El Karim (1991), Mapping of ground water losses by evaporation in the Western Desert of Egypt, Rep. 43, pp. 1 – 116, DLO Winand Staring Cent., Wageningen, Netherlands.
- Monteith, J.L., 1973. *Principles of environmental physics*. Edward Arnold Press. 241 pp.
- Pinker, R. T. (1990), Satellites and our understanding of the surface energy balance, *Paleogr. Palaeoclimatol. Palaeoecol.*, 82, 321–342.

- Price, J. C. (1992), Estimating vegetation amount from visible and near infrared albedo, *Remote Sens. Environ.*, 41, 29–34.
- Qi, J., A. Chehbouni, A. R. Huete, Y. H. Kerr, and S. Sorooshian (1994), A modified soil adjusted vegetation index, *Remote Sens. Environ.*, 48, 119–126.
- Rahman, H., and Dedieu, G., (1994), SMAC: a simplified method for atmospheric correction of satellite measurements in the solar spectrum. *International Journal of Remote Sensing*, 15,123-143.
- Schmugge, T. J., S. Hook, and A. Kahle (1995), TIMS observation of surface emissivity in HAPEX-Sahel, paper presented at International Geoscience and Remote Sensing Symposium, Inst. of Electr. and Electron.Eng., Florence, Italy, July.
- Sellers, P. J., S. I. Rasool, and H. J. Bolle (1990), A review of satellite data algorithms for studies of the land surface, *Bull. Am. Meteorol. Soc.*, 71,1429–1447.
- Sobrino, J. A., and N. Raissouni (2000) Toward remote sensing methods for land cover dynamic monitoring: application to Morocco, *International Journal of Remote Sensing*, 21(2): 353-366.
- Su, Z. (2002), The Surface Energy Balance System (SEBS) for estimation of turbulent heat fluxes, *Hydrol. Earth Syst. Sci.*, 6, 85–99.
- Susskind, J., J. Rosenfield, D. Renter, and M. T. Chahine (1984), Remote sensing of weather and climate parameters from HIRS2/MSU on TIROS-N, *J. Geophys. Res.*, 89, 4677–4697.
- Tanaka K, Ishikawa H, Hayashi T, Tamagawa I, Ma Y (2001) Surface Energy Budget of Amdo on the Eastern Tibetan Plateau using GAME/Tibet IOP98 Data. *Journal of the Meteorological Society of Japan*, 79(1B): 505-517
- Tucker, C. J. (Ed.) (1986), Monitoring the grasslands of semi-arid Africa using NOAA AVHRR data, *Int. J. Remote Sens.*, 7–11, 1383– 1622.
- Wan, Z., and J. Dozier (1989), Land surface temperature measurement from space: Physical principles and inverse modelling, *IEEE Trans. Geosci.Remote Sens.*, 27, 268–278.
- Wang, J., Y. Ma, M. Menenti, W. G. M. Bastiaanssen, and Y. Mitsuata (1995), The

scaling-up of processes in the heterogeneous landscape of HEIFE with the aid of satellite remote sensing, *J. Meteorol. Soc. Jpn.*, 73,1235– 1244.

Watson, K., F. Kruse, and S. Hummer-Miler (1990), Thermal infrared exploration in the Carlin trend, *Geophysics*, 55, 70–79.

Y. Oku, H. Ishikawa (2004), Estimation of Land Surface Temperature over the Tibetan Plateau Using GMS Data, *Journal of applied meteorology*, 43:548-561

Y. Oku, H. Ishikawa, Z. Su, (2007), Estimation of Land Surface Energy Fluxes over the Tibetan Plateau using GMS Data, *J. Appl. Meteorol. Climatol.*,46(2), 183-195

Y. Yamaguchi, A. B. Kahle, H. Tsu, T. Kawakami, and M. Pniel, 1998, Overview of the Advanced Spaceborne Thermal Emission and Reflection Radiometer (ASTER), *Trans. Geosci. Remote Sens.*, vol. 36(4):1062–1071.

Table 1. Ground measurements items in WATER area

Name	Location	Items	Land surface character
Yingke	100°25' E, 38°51' N, 1519 m	wind speed, air temperature and humidity (3 and 10 m), wind direction, air pressure precipitation, four components of radiation, and LST. soil: temperature and moisture profile (10, 20, 40, 80, 120, and 160 cm), and heat flux (5 and 15 cm). EC.	Cropland(maize)
Huazhaizi	100°19' E, 38°46' N, 1726 m	wind speed, air temperature and humidity (2 and 10 m), wind direction, air pressure, precipitation, four components of radiation, and LST. soil: temperature and moisture profile (5, 10, 20, 40, 80, and 160 cm), and heat flux (5 and 15 cm).	Desert steppe
Guantan	100°15' E, 38°32' N, 2835 m	wind speed, air temperature and humidity (2, 10, and 24 m), four components of radiation (1.68 and 19.75 m), wind direction, air pressure, precipitation, snow depth, and PAR. soil: temperature and moisture profile (5, 10, 20, 40, 80, and 120 cm), frost depth, and heat flux (5 and 15 cm). EC, sap flow (3), fall-through, stemflow.	forest
Maliantan	100°18' E, 38°33' N, 2817 m	wind speed, air temperature and humidity (2 and 10 m), wind direction, air pressure, precipitation, and four components of radiation. soil: temperature and moisture profile (5, 10, 20, 40, 80, and 120 cm) and heat flux (5 and 15 cm).	Grassland
A'rou	100°27' E, 38°03' N, 3033m	wind speed, air temperature and humidity (2 and 10 m), wind direction, air pressure, precipitation, and four components of radiation.a soil: temperature, moisture, water potential profile (10, 20, 40, 80, 120, and 160 cm), and heat flux (5 and 15 cm). EC, LAS.	Alpine meadow
Binggou	100°13' E, 38°04' N, 3407m	wind speed, air temperature and humidity (2 and 10 m), wind direction, air pressure, precipitation, and four components of radiation. soil: temperature and moisture profile (5, 10, 20, 40, 80, and 120 cm) and heat flux (5 and 15 cm).	Alpine marshy meadow
Yakou	100°14' E, 38°01' N, 4101 m	wind speed, air temperature and humidity (2 and 10 m), wind direction, air pressure, precipitation, snow depth, and four components of radiation. soil: temperature and moisture profile (5, 10, 20, 40, 80, and 120 cm) and heat flux (5 and 15cm).	Cold desert

Figure captions

Fig. 1 Sketch map of studying area and the sites during the WATER

Fig. 2 Diurnal variations of land surface heat fluxes

Fig. 3 Diagram of parameterization procedure by combining ASTER data with field observations.

Fig. 4 Distribution maps of land surface heat fluxes over the WATER area.

Fig. 5 Validation of the derived net radiation R_n , soil heat flux G_0 , sensible heat flux H and latent heat flux λE against ground measurements over the Watershed Allied Telemetry Experimental Research (WATER) stations, Yingke, Huazhaizi, Guantan, Maliantan, Arou, Binggou and Yakou with 1:1 line.

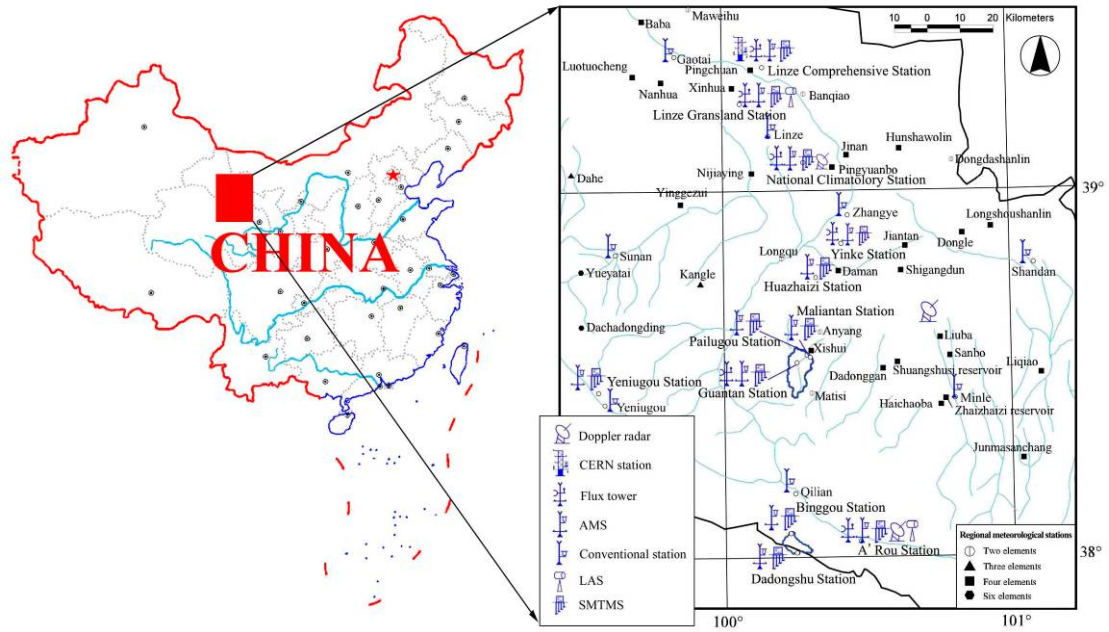


Fig. 1 Sketch map of studying area and the sites during the WATER

Network of the automatic meteorological stations and flux towers in WATER (For regional meteorological stations, two elements indicate air temperature and precipitation; three elements indicate wind direction plus two elements; four elements indicate wind speed plus three elements; six elements indicate air pressure, global radiation plus four elements. SMTMS: Soil Moisture and Temperature Measurement System)

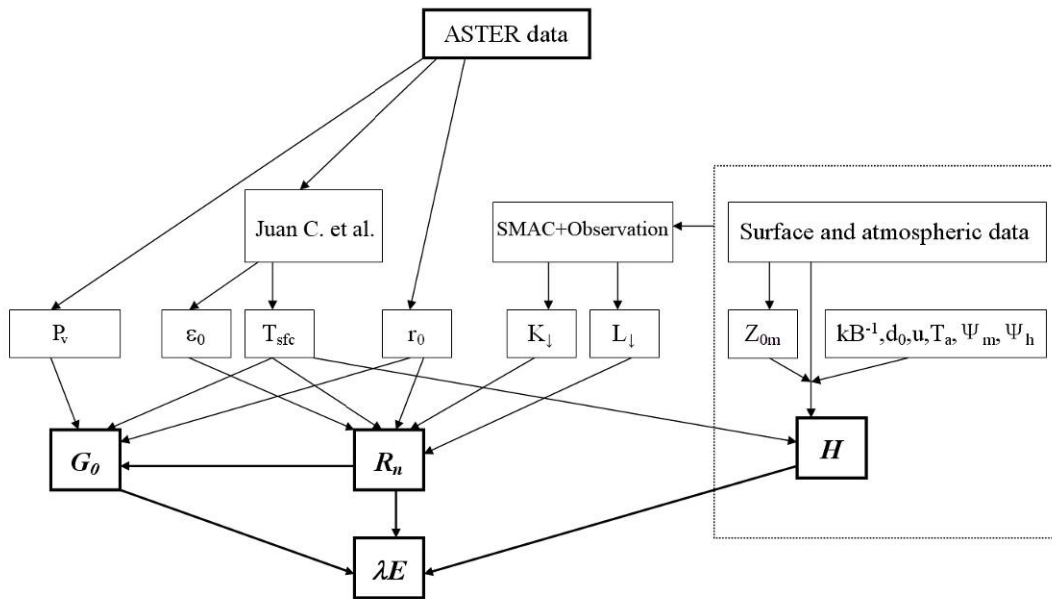


Fig. 2 Diagram of parameterization procedure by combining ASTER data with field observations.

(P_v is vegetation coverage and kB^{-1} is the excess resistance for heat transportation.)

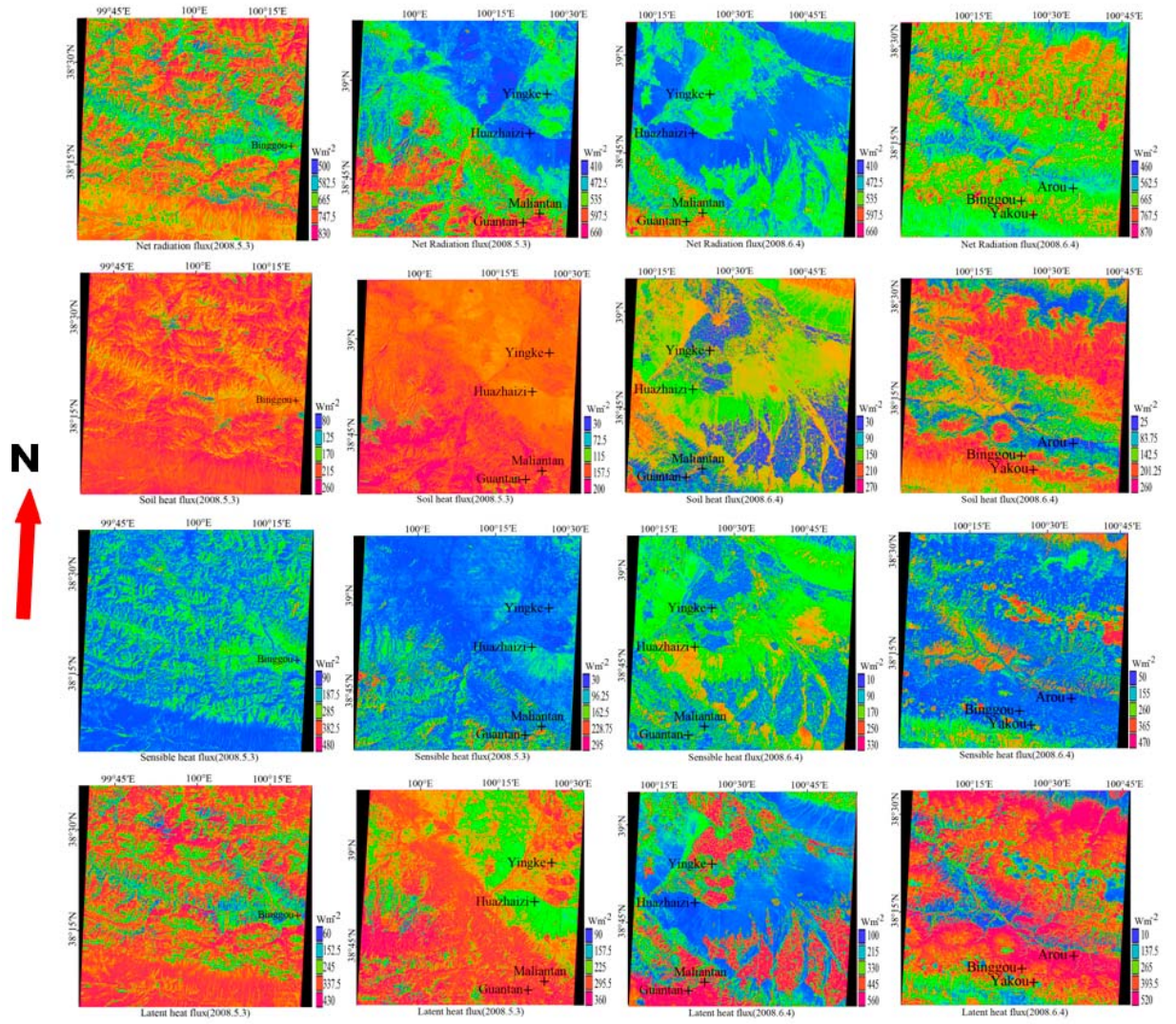


Fig. 3 Distribution maps of land surface heat fluxes over the WATER area

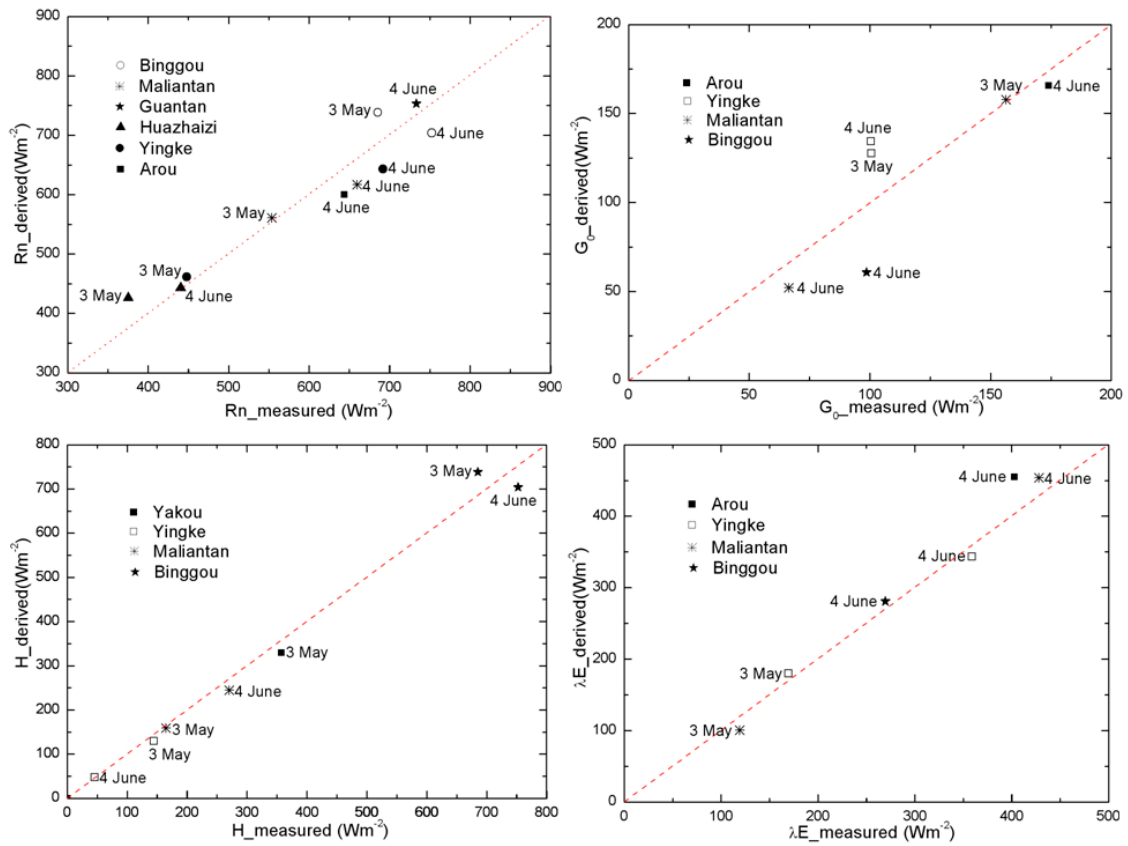


Fig. 4 Validation of the derived net radiation R_n , soil heat flux G_0 , sensible heat flux H and latent heat flux λE against ground measurements over the Watershed Allied Telemetry Experimental Research (WATER) stations, Yingke, Huazhaizi, Guantan, Maliantan, A'rou, Binggou and Yakou with 1:1 line.